Research Article

Song Gao, Shunli Ban, Hao Wang, Dongyi Lei*, and Yaoyao Gong

The influence of oiled fiber, freeze-thawing cycle, and sulfate attack on strain hardening cement-based composites

https://doi.org/10.1515/rams-2022-0023 received October 24, 2021; accepted January 31, 2022

Abstract: The interfacial transition zone (ITZ) between the fiber and the matrix significantly influences the strengthening and toughening effect of the fiber for the matrix. The ITZ between the fiber and mortar is a weak link in strain hardening cementitious composites (SHCC), the loose structure is easily damaged, and it is the main channel of ion attack. The oil reduces the hydrophilicity of fiber and the bonding strength of fiber and mortar, which decreases flexural and compressive strengths, but increases the tensile ductility. The compressive strength increased with the increase in the microhardness of ITZ. Both freeze-thawing cycle and sulfate attack reduce the flexural and compressive strengths, and ductility of SHCC. The failure of ITZ is responsible for the performance decrease. The strength of the samples containing oiled fiber after the freeze-thawing cycle and sulfate attack decreases more significantly.

Keywords: Strain hardening cementitious composite, interfacial transition zone, fiber, mechanical properties, microstructure

Song Gao: School of Civil Engineering, Qingdao University of Technology, Qingdao, 266011, China; Collaborative Innovation Center of Engineering Construction and Safety in Shandong Blue Economic Zone, Qingdao Technological University, Qingdao 266033, China

Shunli Ban, Hao Wang, Yaoyao Gong: School of Civil Engineering, Qingdao University of Technology, Qingdao, 266011, China

International License.

1 Introduction

At present, concrete is still a well-used construction material. However, cement hydration products' heterogeneous structure and characteristics result in making the concrete fragile and prone to crack [1], thereby making the reinforced concrete structure often work with cracks, jeopardizing the durability of concrete structures [2-4]. To address the brittleness issue, fiber is often added to bridge cracks and increase the energy absorption of the material [5]. Among different kinds of fiber-reinforced composites (FRC), strain hardening cementitious composites (SHCC) have stood out with their unique multiple cracking behavior and ultra-high ductility [6-12]. SHCC is designed by micromechanics and fracture mechanics [13-16], which has better toughness, impact resistance, multi-fracture extension, and a high ultimate tensile strain value of up to 3-5% [17]. Benefitting from the fiber bridging cracks, the force transmission property of the SHCC is not significantly weakened by the micro-cracks, which effectively reduces the inherent defects such as fragility and strain softening of concrete [18-23].

A water film is generated between the fibers and mortar during SHCC hardening, while Ca(OH)₂ crystals produced by cement hydration accumulate in the water film layer, creating the interfacial transition zone (ITZ) between the fiber and mortar [24]. The ITZ is often regarded as the "weak link" in a material. The relatively high porosity in the ITZ will provide a more accessible pathway for the aggressive ions to penetrate [25]. Many scholars have conducted theory and engineering application research on the ITZ. Feng et al. [26] investigated the effect of silica fume on the ITZ between steel fibers and matrix, and the microstructure of the ITZ was evaluated using scanning electron microscopy (SEM). The results showed that incorporating silica fume reduced the ITZ breadth and improved the micromechanical properties. Rocha Ferreira et al. [27] used SEM and X-ray diffraction to evaluate the effect of carboxyl styrene-butadiene

^{*} Corresponding author: Dongyi Lei, School of Civil Engineering, Qingdao University of Technology, Qingdao, 266011, China; Postdoctoral Workstation, Guangdong Dongpeng Holding Company Limited, Guangdong, 528031, China, e-mail: leidongyi@qut.edu.cn, dongge0379@126.com

rubber coating on the performance of the vegetable fiber. The results showed that the interaction between the polymer and natural fibers depends on the cellulose amount of fibers and their crystallinity. Hong et al. [28] studied the microstructure and bonding properties of the ITZ in fiber-reinforced concrete. The results showed that many micro-cracks presented in the fiber-mortar ITZ and the content of hydration products were much lower than that in the matrix.

Actual engineering structures are often subjected to harsh environments, such as sulfate attack and freezethawing cycle, but few studies have reported the effects of freeze-thawing cycle and sulfate attack on the structure of ITZ and mechanism of SHCC. Therefore, this article focuses on observing the effects of service environment and oiled fiber on the SHCC's ITZ, combined with fiber-interface indicators to determine the connection between the microstructure and macroscopic properties.

2 Experiment

2.1 Materials

- (1) Cement: P·O 42.5 grade Portland cement. The physical properties are shown in Table 1.
- (2) Fine aggregate: the fine aggregate is river sand produced in Pingdu, Qingdao with fineness modulus of 2.5.
- (3) PVA fiber: the REC15 type PVA fiber is from Japan Kuraray company, the performance index is shown in Table 2.
- (4) Fly ash and slag were used as admixtures, the chemical compositions are presented in Table 3.

2.2 Mix proportion

The mass proportion of cement, slag, fly ash, fine aggregate, water, and PVA fiber in SHCC is 2:1:1:2:1.61:0.098, the water-binder ratio is 0.4, the specific mixing ratio is shown in Table 4. The specific treatment and experiment schemes are shown in Table 5. The sample preparation and performance test are shown in Figure 1.

2.3 Methods of testing

2.3.1 Oil treatment scheme

The oil bath was prepared with the oil and deionized water by the liquor ratio of 1:15 in a beaker. The mixing was carried out with a magnetic stirrer for 5 min at 60°C. After that, PVA fibers were added to the beaker and soaked for 30 min. This allows the oiling agent to deposit on the fiber surface as thin films. Later, the samples were padded at a pressure of 0.2 MPa on a padding machine (one dip, one nip). Finally, the oiled fibers were dried in an oven at 65°C for 30 min.

2.3.2 Mechanical test

GB/T17671-1999 "method of testing cements-Determination of strength" was used to determine the flexural and compressive strengths of SHCC after 28 days curing. The sample size is $40 \text{ mm} \times 40 \text{ mm} \times 160 \text{ mm}$.

2.3.3 Measurement of microhardness

The specimens for the ITZ microhardness test were cut into slices of $40 \, \text{mm} \times 40 \, \text{mm} \times 10 \, \text{mm}$. The slices

Table 1: Cement performance index

Normal consistency (%)	Fineness modulus (%)	Setting time (min)		Compress	ive strength (MPa)	Flexural strength (MPa)	
		Initial	Final	3 days	28 days	3 days	28 days
26	2.5	185	235	18.7	47.9	4.6	7.2

Table 2: PVA fiber performances

Diameter (µm)	Elastic modulus (GPa)	Tensile strength (MPa)	Elongation (%)	Density (g⋅cm ⁻³)	Length (mm)
31	40	1,600	6	1.3	6

Table 3: Chemical composition of fly ash and slag (%)

Oxide	CaO	SiO ₂	Al ₂ O ₃	Fe ₂ O ₃	S 0₃	MgO	TiO ₂
Fly ash							
Slag	35.8	34.5	16.1	0.97	2.25	7.6	1.12

Table 4: The mixture ratio of SHCC (kg·m⁻³)

Cement	Cement Slag Fly ash		Fine aggregate	Water	PVA
533.5	266.7	266.7	533.5	429.5	26.2

Table 5: Experiment scheme

Group	Treatment	Service environment
B ₁	Untreated	Standard curing
B_2	Untreated	Freeze-thawing
B_3	Untreated	Soak for 7 days
B ₄	Untreated	Soak for 60 days
O_1	Oiled	Standard curing
02	Oiled	Freeze-thawing
03	Oiled	Soak for 7 days
O_4	Oiled	Soak for 60 days

Note: B and O represent the specimens containing the untreated fiber and the oiled fiber, respectively. 1, 2, 3, and 4 represent the conditions being original for maintenance, subjected to freezethawing cycle, sulfate attack for 7 days, and sulphate attack for 60 days, respectively.

containing the ITZ between fiber and the matrix were polished with 600# sandpaper and then with 1500# sandpaper to obtain an adequately smooth surface. The HX-1000T microhardness tester measured the microhardness of ITZ. Due to the low microhardness of fiber, the indentation area is too large. The test was performed at 20 μm from the fiber, and the average microhardness is calculated from 10 tests. The Microhardness test is shown in Figure 2.

2.3.4 Tensile test

An electronic universal mechanical testing machine is used to load the sample. The sample is in the shape of dog-bone as shown in Figure 3(a), the loading device is shown in Figure 3(b), and the loading rate is 0.1 mm·min⁻¹.

2.3.5 Freeze-thawing cycle and aggressive ions attack experiments

The number of freeze-thawing cycle was 150 times. The test blocks were immersed in $5\%~Na_2SO_4$ solution for 7 days or 60 days, and the solution was replaced every 15 days to ensure that the PH value of the solution remained constant.

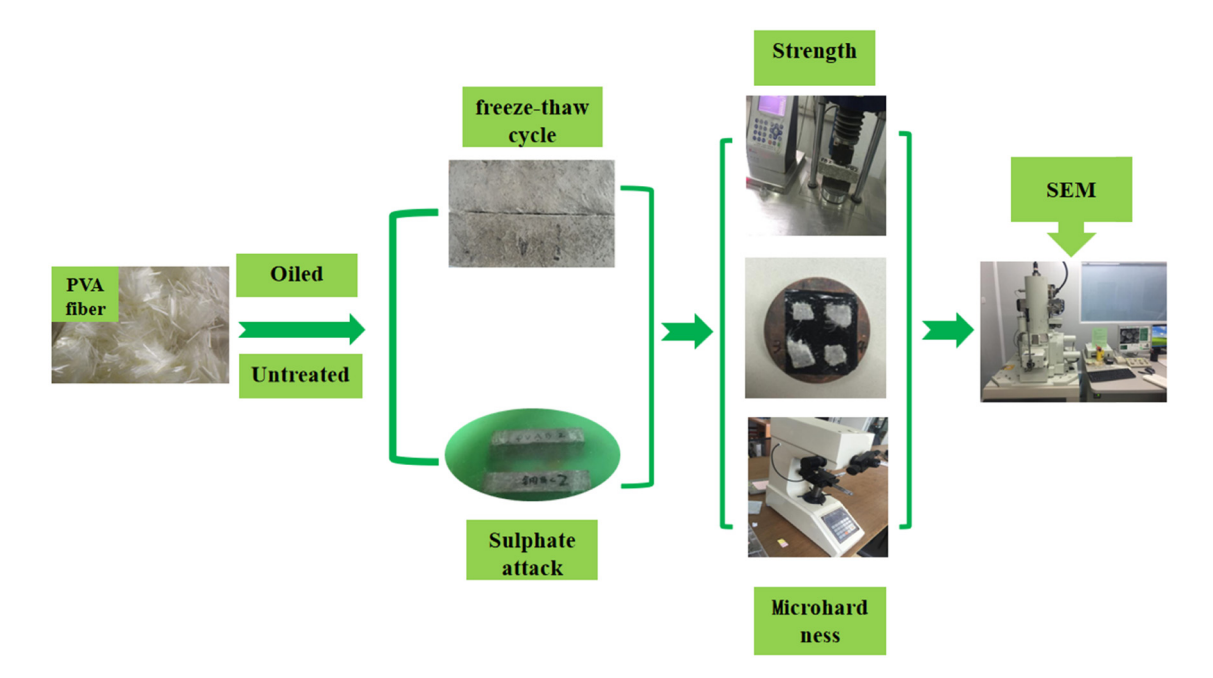


Figure 1: SHCC sample preparation and performance test.

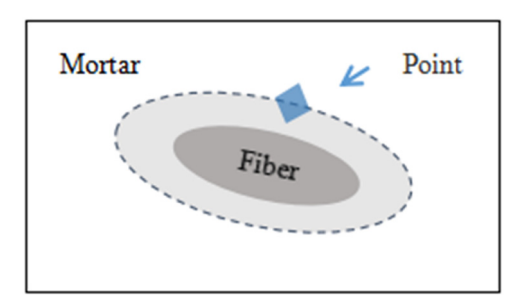


Figure 2: Schematic diagram of microhardness.

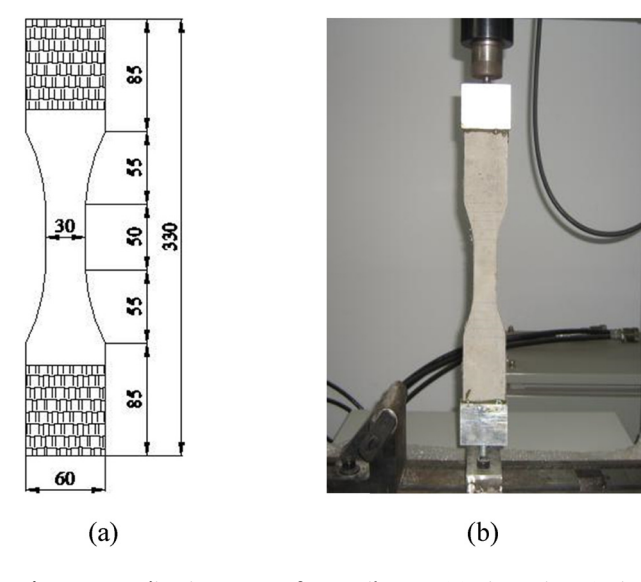


Figure 3: Loading instrument for tensile test. (a) Dimensions (units: mm) of dog-bone shaped specimens and (b) loading device.

3 Results and discussion

3.1 Effects of oiled fiber, freeze-thawing cycle, and sulfate attack on mechanical properties

The change in fiber hydrophilicity and service environment will change the bonding properties between the fiber and mortar, which will affect the interfacial transition zone of SHCC and impact the mechanical properties. Therefore, before studying the ITZ, the effects of oiled fiber, freeze-thawing cycle, and sulfate attack on the mechanical properties of SHCC were analyzed, as shown in Table 6.

Oiled fiber significantly reduced the flexural and compressive strengths of SHCC. The reason is that the oiled fiber reduces the hydrophilicity of the fiber, making

Table 6: The compressive and flexural strengths of SHCC

Group	Flexural strength (MPa)	Compressive strength (MPa)
B ₁	17.4 ± 0.72	51.0 ± 2.1
B_2	14.4 ± 0.51	42.3 ± 1.7
B_3	18.3 ± 0.57	53.3 ± 2.5
B ₄	14.7 ± 0.63	43.9 ± 0.9
O_1	14.4 ± 0.71	40.4 ± 1.4
02	12.7 ± 0.49	38.0 ± 1.9
03	15.9 ± 0.52	43.5 ± 2.3
04	11.7 ± 0.55	37.1 ± 1.1

the hydration products challenging to adhere to the fiber surface, reducing the friction and mechanical bite force between the fiber and the mortar, so, the strength is reduced [7]. The flexural and compressive strengths of SHCC first increase and then decrease with the increase in the sulfate attack age. This may be because of the formation of massive expansive products in the environment of sulfate attack. The products fill the porosity to make the ITZ denser, increasing the early strength [29]. However, when the stresses generated by the expansive products exceed the tensile strength of SHCC, the cracks expand, which destroys the internal structure of SHCC and leads to a decrease in strength [30]. The flexural and compressive strengths of O₄ specimens is lower than O₁ and B₄. This indicates that SHCC with the oiled fiber is more susceptible to damage and has more significant strength loss under sulfate attack.

After 150 freeze-thawing cycles, the flexural strength of the SHCC decreased, and the flexural strength of O2 was lower than B_2 . The main reason is a strong affinity between the unoiled fiber and mortar, which reduces the surface peeling when damaged [31]. However, the bonding strength between the oiled fiber and mortar becomes smaller, so the breaks are more severe when subjected to freeze-thawing cycle damage.

3.2 The influence of oiled fiber, freezethawing cycle, and sulfate attack on tensile properties

The uniaxial tensile stress-strain curve of SHCC is shown in Figure 4. Comparing the specimens with untreated fiber, finding that the SHCC under standard curing presents the strain hardening characteristics, the stress jitter is gentle and shows multiple cracking phenomena. After sulfate attack and freeze-thawing cycle, the tensile

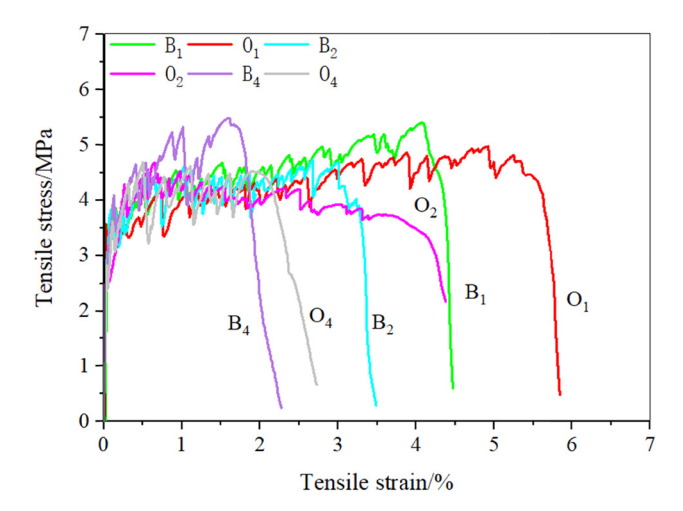


Figure 4: Tensile stress-strain curves of SHCC.

deformation capacity and jitter of the stress–strain curve decreases. However, the specimens after freeze-thawing cycle still exhibit strain hardening characteristics [32,33]. Different from the flexural and compressive strengths, oiled fiber enhances the tensile ductility of SHCC. The ultimate strain is up to 5.4% for original specimens which is significantly higher compared to that of sulfate attack and freeze-thawing cycling specimens, but the ultimate tensile strength decreases.

3.3 Influence of oiled fiber and sulfate attack on microhardness

The influence of oiled fiber and sulfate attack on the microhardness of ITZ is shown in Figure 5(a). Because the samples in the freeze-thawing cycle are severely

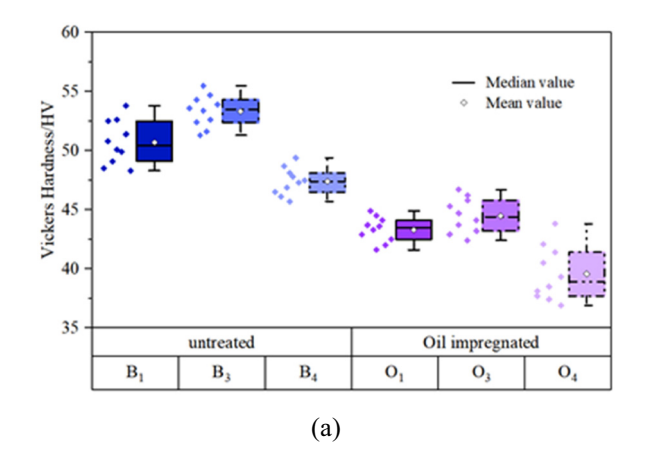
damaged, the freeze-thawing specimens are not analyzed for microhardness.

Under sulfate attack, the microhardness first increases then decreases with the attack age. The reason is that the sulfate first attacks SHCC from ITZ and diffuses into ITZ, making the structure denser, leading to an increase in microhardness. However, when the swelling stress exceeds the tensile strength, causing cracking, spalling, and strength loss in ITZ [34,35], the microhardness decreases. Subsequent Section 3.4 will further analyze the microstructure changes in ITZ and the attack channel of sulfate into SHCC. Oiled fiber reduces the microhardness of SHCC, indicating that the de-hydrophilic treatment for fiber reduces the bonding force between the fiber and the mortar, resulting in a decrease in ITZ hardness.

The best-fitting line of compressive strength and average microhardness is shown in Figure 5(b). The microhardness and compressive strength of SHCC are linearly correlated. The compressive strength increases with the microhardness, indicating that it is necessary to study the interfacial properties of SHCC and ITZ microhardness which are the main factors affecting the mechanical properties of SHCC.

3.4 Micro-morphology of ITZ

The ITZ of SHCC is not only different from mortar in microstructure but also in chemical composition. To more accurately analyze the influence of oiled fiber, freeze-thawing cycle, and sulfate attack on ITZ, the SEM technology was used to observe the interface morphology. The energy dispersive spectroscopy (EDS) technology was used to



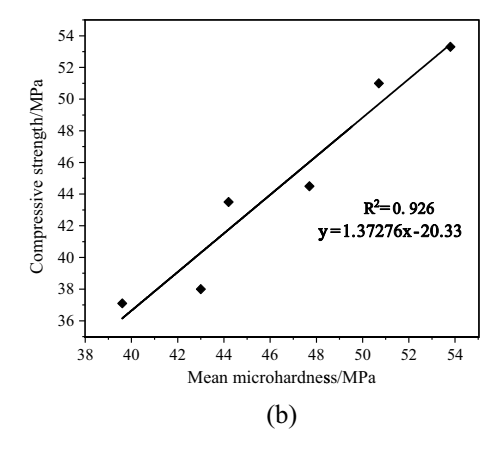


Figure 5: Microhardness and its relationship with compressive strength. (a) Microhardness and (b) the relationship curve between compressive strength and microhardness.

analyze the element changes in SHCC to explore the difference between the hydration products.

3.4.1 The effect of oiled fiber on the ITZ

As exhibited in Figure 6, the mortar completely covered the fibers without exposing the fiber surface, indicating that the untreated fibers have a solid hydrophilic and considerable bonding strength with mortar. Figure 6(b) shows that the ITZ is broken when the fiber is pulled out, indicating that ITZ is weaker than mortar and has a loose structure, often as the cracks' origin. As shown in Figure 7, there is an oil film on the fiber surface, and the friction is slight, which is not enough to bring out the loose structure. The ITZ is relatively intact. There is no apparent rupture or collapse mark, consistent with its ductility.

Using EDS technology to analyze the element composition of the ITZ and mortar of B_1 specimen and O_1 specimen, the location in the B_1 is shown in Figure 8, and the element content is displayed in Figure 9 and Table 7.

Both B_1 and O_1 specimens in ITZ have a higher Ca element and O element content than the mortar, while the Si content is lower than the mortar, indicating that the ITZ is an enriched zone of $Ca(OH)_2$, but it is a poor zone of C-H-S. $Ca(OH)_2$ has a layered structure and weak bonding strength. Once subjected to stress, it is often the origin of cracks, so the ITZ is more easily destroyed. The difference in element content between B_1 and O_1 specimens is slight, so it can be inferred that the oiled fiber only changes the hydrophilicity of the fiber and does not reduce the hydration products. The main reason for the decrease in the compressive and flexural strengths is that the oil decreases the adhesion between mortar and fiber.

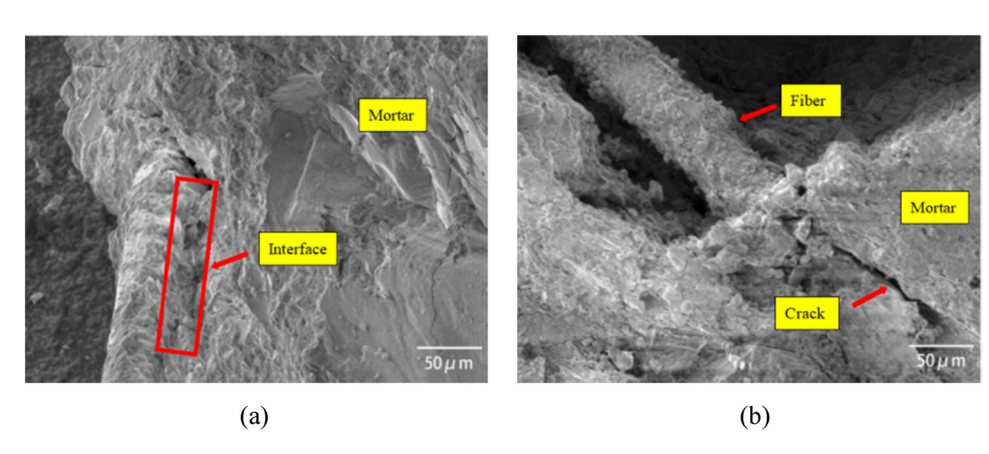


Figure 6: The SEM images of PVA fiber in B₁ specimen. (a) Fiber surface and (b) fiber port.

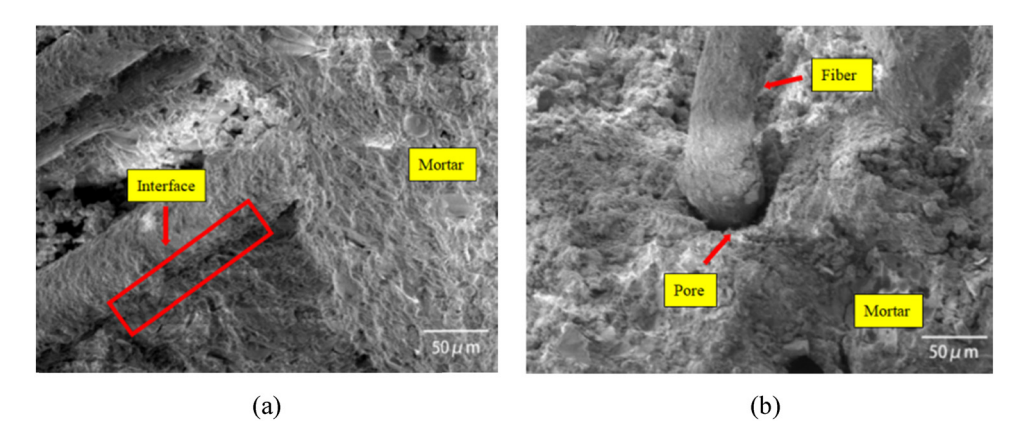


Figure 7: The SEM images of PVA fiber in O₁ specimen. (a) Fiber surface and (b) fiber port.



Figure 8: The location of the groove left by pullout fiber and mortar in B_1 specimen.

3.4.2 The effect of freeze-thawing cycle on ITZ

Figures 10 and 11 show the effects of freeze-thawing cycle on the ITZ. As shown in Figure 10, after the freeze-thawing cycle, the ITZ is looser, more pores, and cracks extend to the mortar. The main reason is that the freeze-thawing cycle makes the toughness of mortar worse, the volume of water film attached to the fiber surface and the free water in the mortar constantly change, which increase the pores between the fiber and the mortar, making the ITZ structure become loose [36].

As exhibited in Figure 11, comparing the B_2 and O_2 specimens, the fiber surface is smooth in O_2 specimen,

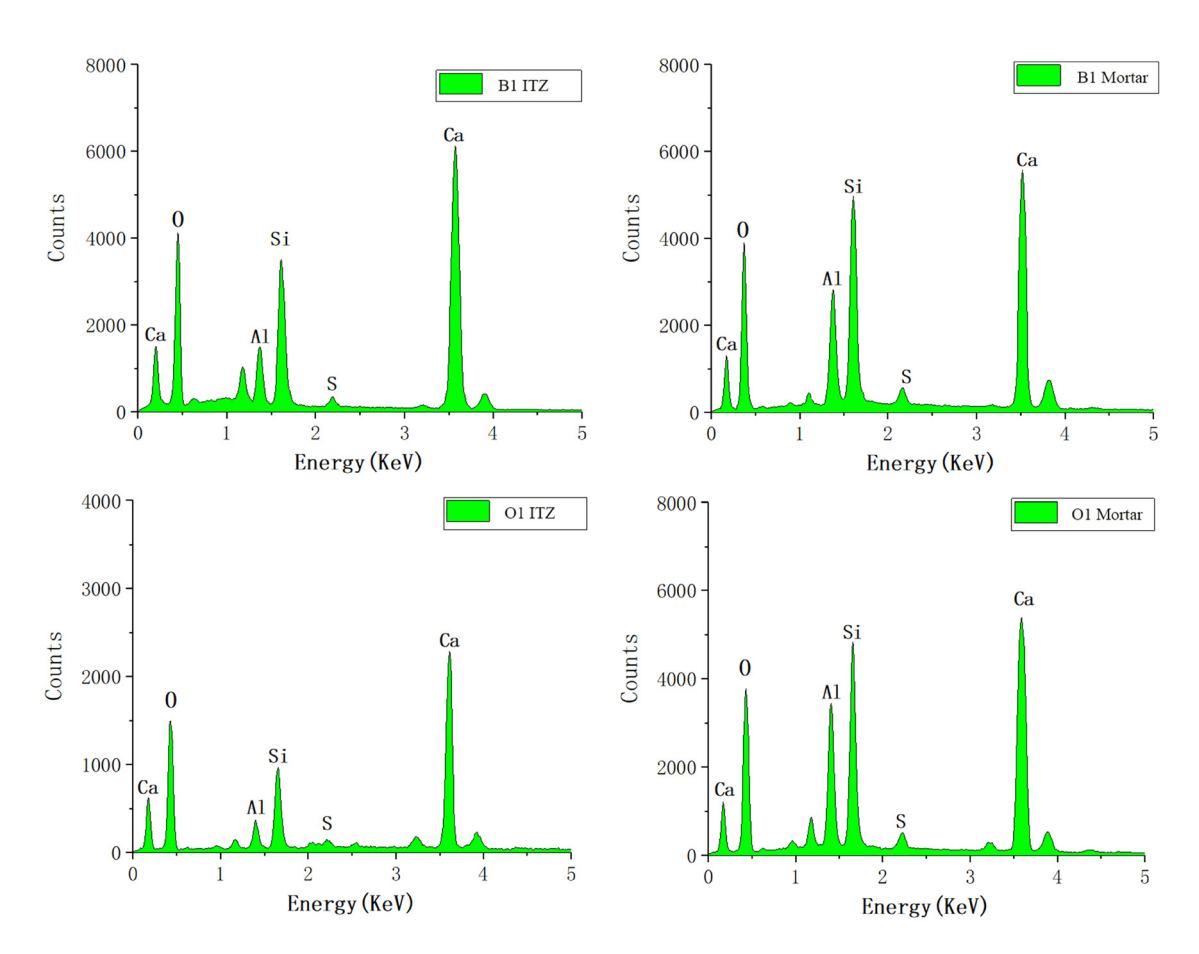


Figure 9: Energy spectra from Element analysis.

Table 7: Element composition of specimens from EDS analysis

Group	Content/% (mass ratio)										
	ITZ					Mortar					
	0	Al	Si	S	Ca	0	Al	Si	S	Ca	
B ₁ O ₁	66.41 64.35	2.29 1.79	5.29 6.54	0.27 0.44	25.74 26.88	62.55 61.66	5.20 5.67	10.32 9.06	0.47 0.77	21.46 22.84	

and the ITZ structure is loose and porous, which reveals that the freeze-thawing cycle destroys the ITZ structure and reduces the bonding strength between the fiber and mortar. Oiled fiber has less bonding strength after freezethawing cycle.

Using EDS technology to analyze the elemental composition of the ITZ and mortar in B2 specimen and O2 specimen, the element content is shown in Figure 12 and Table 8.

The ITZ in B₂ and O₂ specimens with high Ca and low Si content further proves that ITZ is the weak link in SHCC. The element types for B₁, B₂, and O₂ specimens are similar, indicating that the source of freeze-thawing damage is the volume change when water turns into ice, and the hydration product types of ITZ do not change.

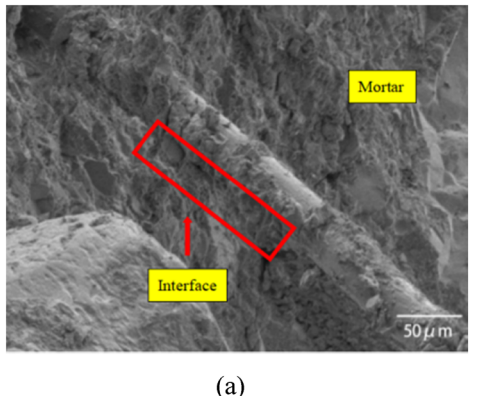
3.4.3 The influence of sulfate attack on the ITZ

The microstructure of the ITZ by sulfate attack for 7 days and 60 days is shown in Figures 13 and 14.

Figures 13 and 14 show that there are many hydration products on the surface of the fibers after sulfate attack for 7 days. Compared with the specimens without sulfate attack, the structure is denser, and products produced by sulfate attack fill the loose system and improve the denseness of ITZ. While the specimens with sulfate attack for 60 days had less adhesion on fiber surface, and the system is more flexible. This shows that the long-term sulfate attack reduces the drawing property of fiber, resulting in decreased flexural strength, compressive strength, and ductility for SHCC. Oiled fiber reduces the bonding strength between the fiber and mortar, making the fiber surface smoother.

EDS technology was used to analyze the element composition of the ITZ and mortar in B_4 and O_4 samples. The element content is shown in Table 9.

Energy spectrum analysis shows that the S content in ITZ is significantly higher than that in the mortar, indicating that the ITZ is the primary way for sulfate attack to invade SHCC, and the sulfate ions first invade the ITZ in SHCC.



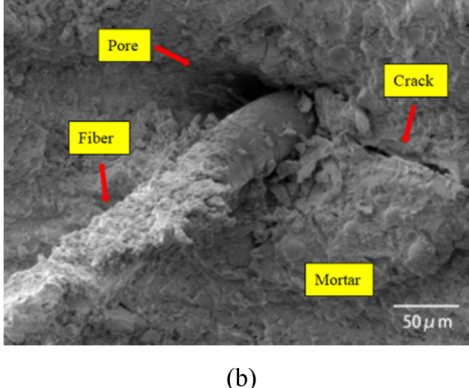
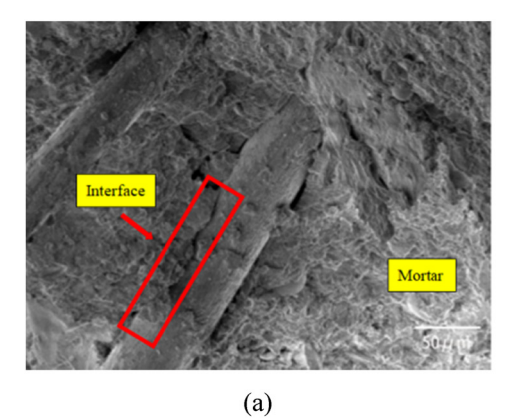


Figure 10: The SEM images of PVA fiber in B2 specimen. (a) Fiber surface and (b) fiber port.



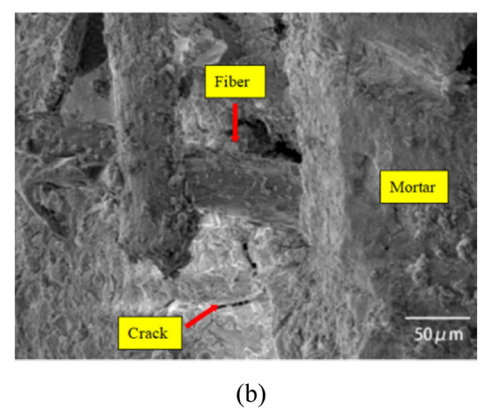


Figure 11: The SEM images of PVA fiber in O₂ specimen. (a) Fiber surface and (b) fiber port.

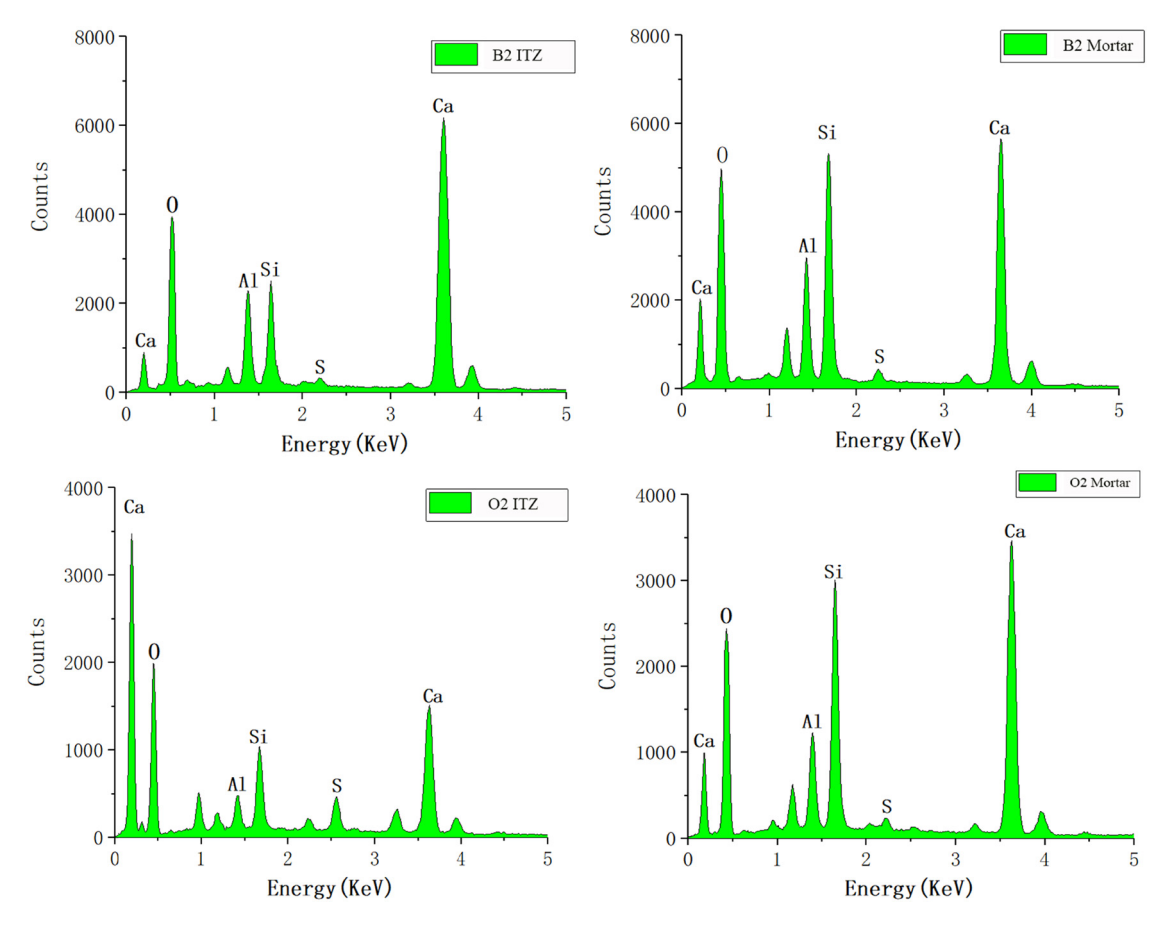


Figure 12: Energy spectra from element analysis.

Table 8: Element composition from EDS analysis

Group	Content/% (mass ratio)										
	ITZ					Mortar					
	0	Al	Si	S	Ca	0	Al	Si	S	Ca	
B ₂ O ₂	63.97 66.06	4.19 2.08	4.36 5.04	0.36 0.81	27.12 26.01	64.69 63.47	3.50 3.60	10.06 9.50	0.40 0.51	21.35 22.92	

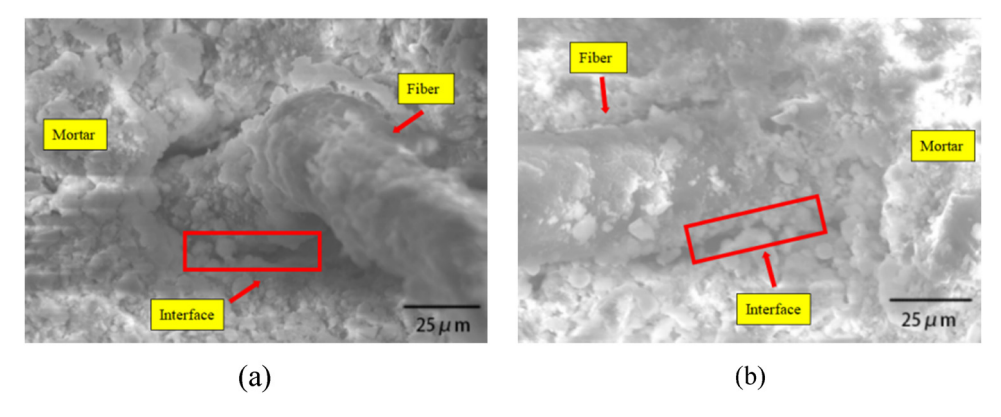


Figure 13: The SEM images of PVA fiber after sulfate attack for 7 days. (a) Untreated and (b) oiled.

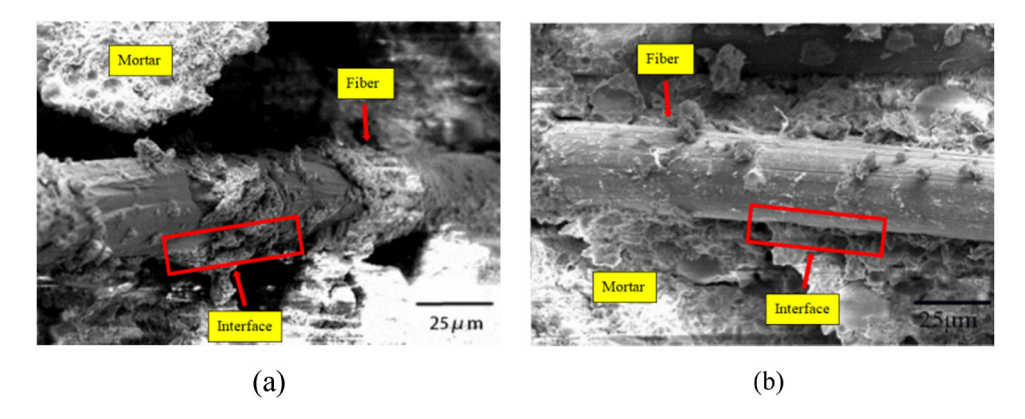


Figure 14: The SEM images of PVA fiber after sulfate attack for 60 days. (a) Untreated and (b) oiled.

Table 9: Element composition of specimens by EDS analysis

Group	Content/% (mass ratio)									
	ITZ					Mortar				
	0	Al	Si	S	Ca	0	Al	Si	S	Ca
B ₄ O ₄	66.30 68.20	3.32 1.38	4.75 6.13	2.19 2.23	23.44 21.26	62.32 63.50	3.10 3.35	8.33 7.47	1.21 1.48	25.04 24.42

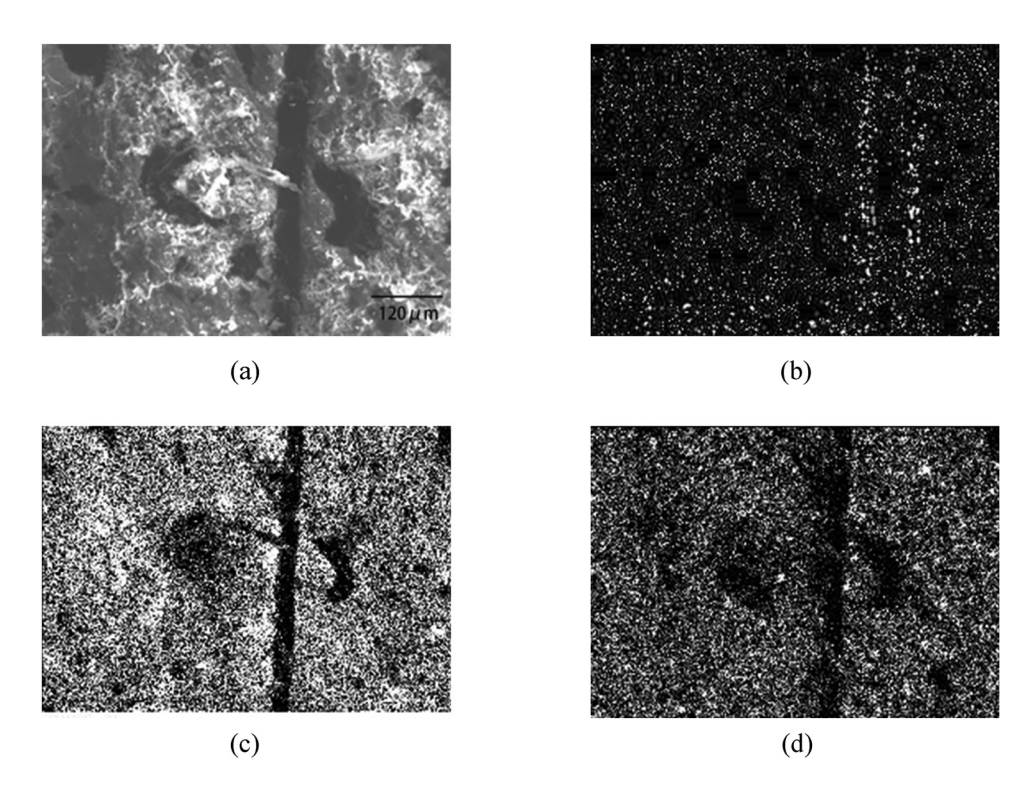


Figure 15: Distribution diagram of the element. (a) EDS mapping-scanning of B_4 specimen, (b) S K α 1, (c) Ca K α 1, and (d) Si K α 1.

To further prove the intrusion path of sulfate attack in SHCC, the ITZ in B₄ specimen was analyzed by EDS mapping-scanning, and the results are shown in Figure 15.

The groove in SEM is the ITZ in SHCC. The content of the S element in ITZ is significantly higher than mortar, and the element distribution is denser. It shows that the sulfate attack is more likely to first invade the ITZ in SHCC. The ITZ is the primary channel for sulfate attack.

In summary, ITZ between fiber and mortar is a weak link in SHCC, an enriched zone containing Ca(OH)₂, which results in main channel of ion attack. The oil reduces the hydrophilicity of fiber, reduces the interaction of fiber-matrix, which decreases flexural and compressive strengths, but lowers the threshold for crack initiation and increases the tensile ductility. Freeze-thawing cycle and sulfate attack for 60 days destroy the ITZ structure, reduce the fiber-mortar bonding strength, which is the main reason for the decrease in the flexural and compressive strengths.

4 Conclusion

The influence of oiled fiber, freeze-thawing cycle, and sulfate attack on the flexural and compressive strengths and flexibility of ITZ between the fiber and mortar of SHCC were studied, and the main conclusions are below:

- (1) The flexural and compressive strengths of SHCC is related to the bonding strength between the fiber and mortar. The greater the friction bonding strength between the fiber and mortar, the higher the mechanical properties for SHCC. The oiled fiber reduces the fiber hydrophilicity, decreasing flexural and compressive strengths, but increases the tensile ductility. Oiled fiber mitigates the microhardness of ITZ. The microhardness increases first and then decreases with an increase in the sulfate attack age.
- (2) The ITZ between fiber and mortar is the weak link in SHCC, the structure is loose and prone to damage, usually the origin of cracks. The EDS results show that the Ca(OH)₂ content of ITZ is higher than that of mortar, but C-H-S content is lower than mortar. Moreover, ITZ is the primary channel for sulfate attacks, so ITZ is more likely to cause performance damage.
- (3) Sulfate attack and freeze-thawing cycle reduce the flexural strength, compressive strength, and ductility of SHCC. Microscopic analysis shows that ITZ damage between fiber and mortar is the main reason for declining performance. Oiled fiber increases the

ductility of the sample subjected to freeze-thawing cycle and sulfate erosion, but the strength decreases. The strength of the samples containing oiled fiber after freeze-thawing cycle and sulfate attack reduces more significantly.

Acknowledgments: The authors would like to acknowledge all the members of Mr. Song Gao's team for their advice and assistance.

Funding information: This work was supported by the National Natural Science Foundation of China (51978353 and 52008223), the Natural Science Foundation of Shandong Province (ZR2020QE252), the China Postdoctoral Science Foundation (2021M700874), the Open Fund of the State Key Laboratory of High-Performance Civil Engineering Materials (PM321022), the Open Fund of the State Key Laboratory of Green Building Materials (2020GBM05), and the Ningbo 2025 Science and Technology Major Project (2020Z035).

Author contributions: Shun-Li Ban: Writing Original Draft, Conceptualization. Dong-Yi Lei: Writing - Review & Editing, Validation, Investigation. Song Gao: Methodology, Investigation, Data Curation. Hao Wang: Conceptualization, Methodology, Term. Yao-Yao Gong: Writing - Review & Editing, Formal analysis.

Conflict of interest: We declare that we have no financial and personal relationships with other people or organizations that can inappropriately influence our work, there is no professional or other personal interest of any nature or kind in any product, service and/or company that could be construed as influencing the position presented in, or the review of, the manuscript entitled.

References

- [1] Lu, C., J. Yu, and C. K. Y. Leung. Tensile performance and impact resistance of strain hardening cementitious composites (SHCC) with recycled fibers. *Construction and Building Materials*, Vol. 171, 2018, pp. 566–576.
- [2] Hisseine, O. A. and A. Tagnit-Hamou. Characterization and nano-engineering the interface properties of PVA fibers in strain-hardening cementitious composites incorporating high-volume ground-glass pozzolans. *Construction and Building Materials*, Vol. 234, 2020, id. 117213.
- [3] Lei D. Y., L. P. Guo, Y. Li, J. P. Liu, B. Chen, D. X. Li, et al. Micro-mechanical model for ultra-high strength and ultra-high

- ductility cementitious composites (UHS-UHDCC). Construction and Building Materials, Vol. 267, 2020, id. 120668.
- Lei, D. Y., L. P. Guo, Y. Li, Z. Zheng, J. P. Liu, S. C. Li, et al. The investigating on mechanical properties of ultra-high strength and ultra-high ductility cementitious composites (UHS-UHDCC). Journal of Building Engineering, Vol. 43, 2021, id. 102486.
- [5] Aveston, J. and A. Kelly. Theory of multiple fracture of fibrous composites. Materials Science, Vol. 8, 1973, pp. 352-362.
- Li, V. C. and C. K. Y. Leung. Steady-state and multiple cracking of short random fiber composites. Engineering Mechanics, Vol. 118, 1992, pp. 2246-2264.
- [7] Pan, Z., C. Wu, J. Liu, W. Wang, and J. Liu. Study on mechanical properties of cost-effective polyvinyl alcohol engineered cementitious composites (PVA-ECC). Construction and Building Materials, Vol. 78, 2015, pp. 397-404.
- [8] Li, V. C. On engineered cementitious composites (ECC). Advanced Concrete Technology, Vol. 1, 2003, pp. 215-230.
- Lu, Z., D. Hou, L. Meng, G. Sun, C. Lu, and Z. Li. Mechanism of cement paste reinforced by graphene oxide/carbon nanotubes composites with enhanced mechanical properties. RSC Advances, Vol. 5, 2015, pp. 100598-100605.
- [10] Yu, J. and C. K. Y. Leung. Strength improvement of strain-hardening cementitious composites with ultrahigh-volume fly ash. Materials in Civil Engineering, Vol. 29, 2017, id. 05017003.
- [11] Yu, K. Q., J. T. Yu, J. G. Dai, Z. D. Lu, and S. P. Shah. Development of ultra-high performance engineered cementitious composites using polyethylene (PE) fibers. Construction and Building Materials, Vol. 158, 2018, pp. 217-227.
- [12] Chen, Y., J. Yu, and C. K. Y. Leung. Use of high strength strainhardening cementitious composites for flexural repair of concrete structures with significant steel corrosion. Construction and Building Materials, Vol. 167, 2018, pp. 325-337.
- [13] Li, V. C. and H. C. Wu. Conditions for pseudo strain-hardening in fiber reinforced brittle matrix composites. Applied Mechanics Reviews, Vol. 45, 1992, pp. 390-398.
- [14] Lu, C., C. K. Leung, and V. C. Li. Numerical model on the stress field and multiple cracking behavior of engineered cementitious composites (ECC). Construction and Building Materials, Vol. 133, 2017, pp. 118-127.
- [15] Lu, C. and C. K. Leung. A new model for the cracking process and tensile ductility of strain hardening cementitious composites (SHCC). Cement and Concrete Research, Vol. 79, 2016, pp. 353-365.
- [16] Leung, C. K. Y. Design criteria for pseudoductile fiber-reinforced composites. Engineering Mechanics, Vol. 122, 1996, pp. 10-18.
- [17] Arain, M. F., M. Wang, J. Chen, and H. Zhang. Study on PVA fiber surface modification for strain-hardening cementitious composites (PVA-SHCC). Construction and Building Materials, Vol. 197, 2019, pp. 107-116.
- [18] Gao, S., J. Jin, G. Hu, and L. Qi. Experimental investigation of the interface bond properties between SHCC and concrete under sulfate attack. Construction and Building Materials, Vol. 217, 2019, pp. 651-663.
- [19] Kim, M. J., H. J. Choi, W. Shin, T. Oh, and D. Y. Yoo. Development of impact resistant high-strength

- strain-hardening cementitious composites (HS-SHCC) superior to reactive powder concrete (RPC) under flexure. Journal of Building Engineering, Vol. 44, 2021, id. 102652.
- [20] Yu, J., H. Li, C. K. Y. Leung, X. Lin, J. Lam, I. Sham, et al. Sham. Matrix design for waterproof engineered cementitious composites (ECCs). Construction and Building Materials, Vol. 139, 2017, pp. 438-446.
- [21] Yu, J., J. Yao, X. Lin, H. Li, J. Lam, C. Leung, et al. Tensile performance of sustainable strain-hardening cementitious composites with hybrid PVA and recycled PET fibers. Cement and Concrete Research, Vol. 107, 2018, pp. 110-123.
- [22] Curosu, I., M. Liebscher, G. Alsous, E. Muja, H. Li, A. Drechsler, et al. Tailoring the crack-bridging behavior of strain-hardening cement-based composites (SHCC) by chemical surface modification of poly (vinyl alcohol) (PVA) fibers. Cement and Concrete Composites, Vol. 114, 2020, id. 103722.
- [23] Mohammedameen, A., M. E. Gülşan, R. Alzeebaree, A. Çevik, and A. Niş. Mechanical and durability performance of FRP confined and unconfined strain hardening cementitious composites exposed to sulfate attack. Construction and Building Materials, Vol. 207, 2019, pp. 158-173.
- [24] Özbay, E., O. Karahan, M. Lachemi, K. Hossain, and C. D. Atis. Dual effectiveness of freezing-thawing and sulfate attack on high-volume slag-incorporated ECC. Composites Part B: Engineering, Vol. 45, 2013, pp. 1384-1390.
- Fang, G. H. and M. Z. Zhang. The evolution of interfacial transition zone in alkali-activated fly ash-slag concrete. Cement and Concrete Research, Vol. 129, 2020, id. 105963.
- [26] Feng, H., L. Li, P. Zhang, D. Gao, J. Zhao, L. Feng, et al. Microscopic characteristics of interface transition zone between magnesium phosphate cement and steel fiber. Construction and Building Materials, Vol. 253, 2020, id. 119179.
- [27] Rocha Ferreira, S., A. Rodrigues Sena Neto, F. de Andrade Silva, F. Gomes de Souza, and R. Dias Toledo Filho. The influence of carboxylated styrene butadiene rubber coating on the mechanical performance of vegetable fibers and on their interface with a cement matrix. Construction and Building Materials, Vol. 262, 2020, id. 120770.
- [28] Hong, L., Y. D. Chen, T. D. Li, P. Gao, and L. Z. Sun. Microstructure and bonding behavior of fiber-mortar interface in fiber-reinforced concrete. Construction and Building Materials, Vol. 232, 2020, id. 117235.
- [29] Gao, Y., G. D. Schutter, and G. Ye. Micro and meso-scale pore structure in mortar in relation to aggregate content. Cement and Concrete Research, Vol. 52, 2013, pp. 149-160.
- [30] Yue, G., Z. Ma, M. Liu, C. Liang, and G. Ba. Damage behavior of the multiple ITZs in recycled aggregate concrete subjected to aggressive ion environment. Construction and Building Materials, Vol. 245, 2020, id. 118419.
- Yun, H. D. Effect of accelerated freeze-thawing cycling on mechanical properties of hybrid PVA and PE fiber-reinforced strain-hardening cement-based composites (SHCC). Composites Part B: Engineering, Vol. 52, 2013, pp. 11–20.
- [32] Meng, Z., Q. Liu, Y. Zhang, J. Sun, C. Yang, H. Li, et al. Tensile properties of hybrid fiber-reinforced strain-hardening cementitious composite exposed to elevated temperature. Journal of Building Engineering, Vol. 34, 2021, id. 101886.
- [33] Lu, Z. Y., J. Yao, and C. K. Y. Leung. Using graphene oxide to strengthen the bond between PE fiber and matrix to improve

- the strain hardening behavior of SHCC. Cement and Concrete Research, Vol. 126, 2019, id. 105899.
- [34] Li, H., Q. J. Guo, and J. B. Wang. Meso-/Micro-structure of interfacial transition zone and durability of recycled aggregate concrete: a review. *Composites Part B: Engineering*, Vol. 34, 2020, pp. 13050–13057.
- [35] Lu, Z., R. Yin, J. Yao, and C. Leung. Surface modification of polyethylene fiber by ozonation and its influence on the
- mechanical properties of Strain-Hardening Cementitious Composites. *Composites Part B: Engineering*, Vol. 177, 2019, id. 107446.
- [36] Nam, J., G. Kim, and B. Lee. Frost resistance of polyvinyl alcohol fiber and polypropylene fiber reinforced cementitious composites under freeze thaw cycling. *Composites Part B: Engineering*, Vol. 90, 2016, pp. 241–250.